Hindawi Publishing Corporation
Journal of Thermodynamics
Volume 2011, Article ID 251075, 11 pages
doi:10.1155/2011/251075

Research Article

Vapor-Liquid Equilibrium of Carbon Dioxide + Ethanol: Experimental Measurements with Acoustic Method and Thermodynamic Modeling

Ana Mehl,[1] Fabio P. Nascimento,[1] Pedro W. Falcão,[2] Fernando L. P. Pessoa,[1] and Lucio Cardozo-Filho[3]

[1] *Centro de Tecnologia, Escola de Química Bloco E Sl E-201, Federal University of Rio de Janeiro, Avenida Horácio Macedo, 2030, 21941-909 Ilha do Fundão, RJ, Brazil*
[2] *Centro de Tecnologia, COPPE-PEQ-UFRJ, Avenida Horácio Macedo, 2030, Bloco G S-l G-119, 21941-909 Ilha do Fundão, RJ, Brazil*
[3] *Departamento de Engenharia Química, Universidade Estadual de Maringá, Avenida Colombo, 5790, Bloco D-90, 87020-900 Maringá, PR, Brazil*

Correspondence should be addressed to Lucio Cardozo-Filho, cardozodequem@yahoo.com.br

Received 25 November 2010; Revised 22 February 2011; Accepted 15 March 2011

Academic Editor: Felix Sharipov

Phase behavior of systems composed by supercritical carbon dioxide and ethanol is of great interest, especially in the processes involving supercritical extraction in which ethanol is used as a cosolvent. The development of an apparatus, which is able to perform the measurements of vapor-liquid equilibrium (VLE) at high pressure using a combination of the visual and the acoustic methods, was successful and was proven to be suited for determining the isothermal VLE data of this system. The acoustic method, based on the variation of the amplitude of an ultra-sound signal passing through a mixture during a phase transition, was applied to investigate the phase equilibria of the system carbon dioxide + ethanol at temperatures ranging from 298.2 K to 323.2 K and pressures from 3.0 MPa to 9.0 MPa. The VLE data were correlated with Peng-Robinson equation of state combined with two different mixing rules and the SAFT equations of state as well. The compositions calculated with the models are in good agreement with the experimental data for the isotherms evaluated.

1. Introduction

VLE data are usually obtained experimentally through either sampling or visual methods. The sampling at high pressures is a hard task. Moreover, the sampling can cause disturbances in the equilibrium and the sample may not be representative of the desired phase. Compared with the sampling technique, the visual method, which is based on the direct observation of the appearance and disappearance of an interface between the phases, is the most adequate technique [1]. In transparent system phase transitions, such as, bubble point, liquid-liquid separation, and incipient crystallization, can be detected via visual method. However, the detection of critical points is limited and very dependent on the visual interpretation of the observer. The technique also leads to erroneous results when the phases involved in the equilibrium have similar densities.

The visual method is not suitable for opaque systems. In such cases, the phase transition must be determined indirectly through the identification of discontinuities of certain physical properties [2]. For instance, measurements of velocity or decrease of the ultrasonic waves can be used to detect either phase changes or critical points of mixtures [3]. According to the literature, the acoustic method overcomes the disadvantages of both the sampling (analytical) and the visual methods and is applicable to practically all kinds of phase behavior. The detection can be carried out in opaque flasks, and the measurement is direct and totally independent on any visual interpretation from the observer. The transition from liquid to vapor can be easily identified

by the minimum sound velocity observed in the vapor phase [1].

The application of supercritical fluids (SCF) technologies covers fields, such as, food and pharmaceutical, chemical reactions, coal and oil processing, and waste treatment. Carbon dioxide with favorable characteristics, such as small critical temperature, nonflammability, low toxicity, and low price beyond the fact that it is known as a earth-friendly solvent, is a potential solvent for the supercritical extractions especially in food and pharmaceutical industries. However, due to its rather low solvency power, in comparison with common liquid organic solvents, the addition of cosolvents is sometimes required in order to improve the solubility of compounds that exhibit poor miscibility in the supercritical carbon dioxide.

In the synthesis of many pharmaceutical products, the low productivity normally found in the processes which employ SCF is mostly due to the difficulty in achieving a complete water removal from the original aqueous solution. In order to overcome this problem, ethanol can be used as a cosolvent so that the miscibility of supercritical carbon dioxide in water is improved yielding better efficiency for the process. As a result, ethanol becomes an important cosolvent of SCF in bioseparations and, as an example, can be added to supercritical carbon dioxide to separate water from the diluted aqueous solutions generated in biochemical synthesis.

The knowledge of phase equilibrium behavior and solubility in supercritical components is essential for the design of industrial processes involving chemical reactions in either SCF media or supercritical extraction. In the case of the enzymatic ethanolysis of vegetable oils to produce biodiesel in the presence of supercritical carbon dioxide, data of solubility of ethanol, glycerol, triglycerides, and corresponding ethyl esters are required either for the evaluation of the influence of the phase behavior in the kinetics or for the design of the separation process downstream the reactor. Such data are important especially at 318.2 K, which was identified, as the optimal reaction temperature for the performance of the immobilized lipase Novozym 435 [4].

The open literature presents studies on the modifications in the phase behavior of SCF as a result of the use of polar cosolvents [5]. The enhancement of the solubility of palmitic acid in the supercritical carbon dioxide was observed with the addition of ethanol at different temperatures [6].

Regarding the solubility of ethanol in the supercritical carbon dioxide, several VLE experimental data at different temperatures are available in the open literature, but none of them at 318.2 K. VLE data for this system at this temperature can be estimated with proper thermodynamic models, for example, equations of state, if the dependence of the binary interactions parameters, fitted to experimental *P-x-y* data retrieved from the literature, with the temperature being determined. Often empirical expressions relating the parameters with temperature can be obtained by fitting. However, the prediction of the phase equilibrium of a mixture comprising both a supercritical compound and an associating substance at high pressure based simply on empirical correlations of binary interactions parameters with temperature is a not always successful. Unless the temperature range used in the fitting is small, the empirical dependence is not satisfactory. Therefore, it is preferable to measure the VLE data at the specific conditions.

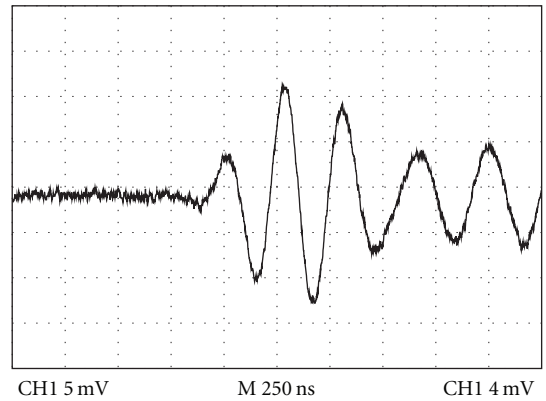

Figure 1: US signal when the system is in the liquid phase.

The open literature presents many studies on use of both the sampling method [7, 8] and the visual technique [9] to investigate the phase behavior of the binary system composed by ethanol and carbon dioxide at temperatures similar to those under investigation in this work.

The main objective of this work was the development of an apparatus, which is able to carry out the measurements of the VLE at high pressure using a combination between the visual and the acoustic methods and determine VLE data of the system carbon dioxide + ethanol at temperatures at a range of 298.2 K to 323.2 K, specifically at 318.2 K, which is new data.

2. Fundamentals of the Acoustic Method

Experimental investigations have demonstrated that the velocity of the ultra-sound (US) wave is highly dependent on the temperature and pressure conditions of the medium in which it passes through. The application of the ultrasonic technique to phase equilibrium measurements is based on the difference of the acoustic impedance observed over the phase changes. The acoustic impedance is defined as the product between the acoustic velocity and the specific mass of the medium. When excited in a liquid sample, an acoustic wave is strongly reduced when the physical state changes from liquid to vapor. Hence, the phase transition can be easily indentified.

In the bubble point, the amplitude of the signal of the US decreases due to the difference of the impedance between the bubble and the bulk liquid. The US wave generated by the transductor propagates through the medium. In the case of liquid under pressure, the amplitude of the signal is maximum. When a bubble shows up the wave gets spread out as a result of the difference in the impedance and the amplitude of the signal reaches a minimum value. Figure 1 shows the US wave image, captured in the oscilloscope, when the system is in the liquid phase. The decrease of the US wave amplitude detected over the phase transition is shown in Figure 2.

Table 1: Bubble pressures of carbon dioxide + ethanol system at 298.2 K.

x_{CO_2} (molar fraction)	P(bubble)/MPa (visual method)	P(bubble)/MPa (acoustic method)
0.2078	2.79	2.79
0.3094	3.89	3.88
0.4117	4.67	4.67
0.5108	5.15	5.14
0.6110	5.44	5.44
0.7093	5.63	5.62
0.8074	5.64	5.64

Table 2: Experimental bubble pressures of carbon dioxide + ethanol at different temperatures.

$x_{C_2H_5OH}$ (molar fraction)	P(bubble)/MPa 313.2 K	P(bubble)/MPa 318.2 K	P(bubble)/MPa 323.2 K
0.1928	7.53 ± 0.2	8.21 ± 0.3	8.89 ± 0.1
0.2905	7.27 ± 0.1	7.97 ± 0.3	8.58 ± 0.1
0.3891	7.14 ± 0.3	7.77 ± 0.2	8.41 ± 0.5
0.4986	6.73 ± 0.6	7.30 ± 0.1	8.03 ± 0.1
0.5890	5.98 ± 0.2	6.44 ± 0.6	6.96 ± 0.6
0.6903	4.74 ± 0.3	5.12 ± 0.3	5.48 ± 0.1
0.7926	3.38 ± 0.1	3.65 ± 0.3	3.88 ± 0.6

Table 3: Pure component parameters of Conventional SAFT and SAFT-ConvexBody.

	SAFT-ConvexBody		SAFT Conventional	
	CO_2	ethanol	CO_2	ethanol
Association scheme	—	1(+) 1(−)	—	1(+) 1(−)
(μ^0/k)/K	274.37	213.87	216.08	215.32447
$v^{00}/(\mathrm{l}\cdot\mathrm{mol}^{-1})$	0.019801	0.012449	0.013578	0.0127124
m	1.000	2.384	1.417	2.4060394
(ε/k)/K	—	2791.2	—	2794.0618
κ	—	0.025819	—	0.0250426
φ/k	52.0	10.0	40.0	10.394176
α	1.056	1.000	—	—

Table 4: Binary interaction parameters for $CO_2(1)$ + ethanol(2) using Conventional SAFT and SAFT-ConvexBody with van der Waals quadratic mixing rule.

	SAFT-ConvexBody		Conventional SAFT	
T/K	k_{12}	λ_{12}	k_{12}	λ_{12}
298.15	0.08275	0.07534	0.06288	0.04132
313.15	0.08065	0.08718	0.06142	0.04634
318.15	0.08089	0.09050	0.06300	0.04958
323.15	0.08204	0.09216	0.06328	0.04953

Table 5: Binary interaction parameters for $CO_2(1)$ + ethanol(2) using PR with van der Waals quadratic and Mathias-Klotz-Prausnitz (MKP) mixing rules.

	PR quadratic		PR-MKP		
T/K	k_{12}	l_{12}	k_{12}	l_{12}	λ_{12}
298.15	0.09536	0.0162	0.46672	0.38592	0.45273
313.15	0.08623	0.00715	0.44474	0.36118	0.45363
318.15	0.08373	0.00245	0.35660	0.27145	0.34872
323.15	0.08447	−0.00047	0.39544	0.31006	0.40172

Table 6: Average relative deviations of liquid CO_2 molar fractions and bubble pressures.

$100 \cdot \sum[\text{abs}(x_{\text{exp}} - x_{\text{calc}})/x_{\text{exp}}]/N_{\text{points}}$				$100 \cdot \sum[\text{abs}(\text{BP}_{\text{exp}} - \text{BP}_{\text{calc}})/\text{BP}_{\text{exp}}]/N_{\text{points}}$			
298.15 K				298.15 K			
PR-MKP	PR quadratic	SAFT ConvexBody	SAFT Conv.	PR-MKP	PR quadratic	SAFT ConvexBody	SAFT Conv.
3.9	6.0	7.4	4.9	2.3	3.6	3.8	2.2
313.15 K				313.15 K			
PR-MKP	PR quadratic	SAFT ConvexBody	SAFT Conv.	PR-MKP	PR quadratic	SAFT ConvexBody	SAFT Conv.
2.9	6.9	8.9	5.8	1.5	4.2	5.2	3.3
318.15 K				318.15 K			
PR-MKP	PR quadratic	SAFT ConvexBody	SAFT Conv.	PR-MKP	PR quadratic	SAFT ConvexBody	SAFT Conv.
2.1	5.1	8.6	5.5	1.9	3.0	5.2	3.3
PR-MKP	PR quadratic	SAFT ConvexBody	SAFT Conv.	PR-MKP	PR quadratic	SAFT ConvexBody	SAFT Conv.
323.15 K				323.15 K			
PR-MKP	PR quadratic	SAFT ConvexBody	SAFT Conv.	PR-MKP	PR quadratic	SAFT ConvexBody	SAFT Conv.
3.8	6.6	9.3	6.2	2.1	4.1	5.7	4.3

Table 7: VLE at 298.2 K.

298.2 K									
Pexp (MPa)		PR-MKP		PR quadratic		SAFT-ConvexBody		Conventional SAFT	
	x_{CO_2}exp	x_{CO_2}calc	y_{CO_2}calc	x_{CO_2}calc	y_{CO_2}calc	x_{CO_2}calc	y_{CO_2}calc	x_{CO_2}calc	y_{CO_2}calc
2.79	0.2078	0.2250	0.9959	0.2365	0.9955	0.1787	0.9965	0.1874	0.9965
3.88	0.3094	0.3264	0.9965	0.3415	0.9960	0.2877	0.9972	0.2972	0.9973
4.67	0.4117	0.4174	0.9966	0.4342	0.9959	0.4154	0.9975	0.0415	0.9976
5.14	0.5108	0.4919	0.9965	0.5081	0.9958	0.5524	0.9977	0.5272	0.9978
5.44	0.6110	0.5680	0.9964	0.5803	0.9956	0.6737	0.9977	0.6452	0.9979
5.62	0.7093	0.7153	0.9964	0.7049	0.9955	0.7416	0.9978	0.7550	0.9979
5.64	0.8074	0.8028	0.9964	0.8573	0.9955	0.7486	0.9978	0.7699	0.9980

x_{CO_2}: liquid phase molar fraction.
y_{CO_2}: vapor phase molar fraction.

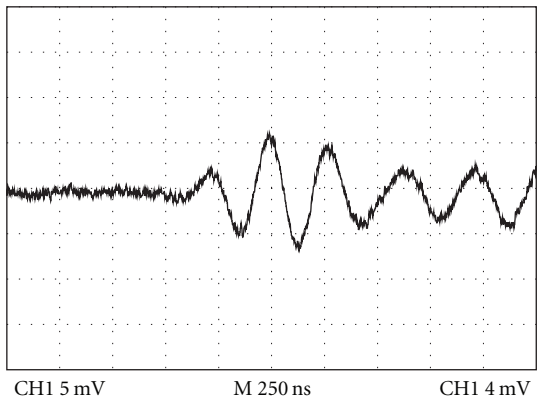

Figure 2: US signal when the system is in the bubble point.

3. Experimental Section

3.1. Materials. Carbon dioxide was supplied by Lynde Gas with a purity of 99.99%, and ethanol 99.9% (with 0.1% water maximum) was obtained from VETEC Química, Brazil. Both chemicals were used without any further purification.

3.2. Equipment and Procedure. The apparatus designed to the measure the bubble points curve, that can support pressure and temperature up to 40.0 MPa and 343 K, respectively, is schematically described in Figure 3.

The high pressure variable volume cell used to perform phase transition measurements by acoustic and visual methods is made of stainless steel. It comprises two main parts: (i) a frontal compartment with flat surfaces to allow the location of the two ulta-sound transducers in two flat walls that are opposed, parallel, and perfectly aligned, and (ii) a cylindric compartment with a mobile piston which pressurizes or depressurizes the mixture. This part contains an obstacle properly located so that the piston cannot penetrate into the frontal compartment.

In the frontal superior part of the cell, there are three nozzles in the cell that are used for temperature indication and control, solvent injection, and pressure measurement. The cell is provided with two sapphire windows. In the frontal window, a video acquisition system consisting of a *webcam* (Logitech Quickcam Orbit AF) connected to a computer allows the observation of the cell interior. The other sapphire window, located in the top, is used for illumination inside the cell.

Table 8: VLE data at 313.2 K.

313.2 K									
*P*exp (MPa)		PR-MKP		PR quadratic		SAFT-ConvexBody		Conventional SAFT	
	x_{CO_2} exp	x_{CO_2} calc	y_{CO_2} calc	x_{CO_2} calc	y_{CO_2} calc	x_{CO_2} calc	y_{CO_2} calc	x_{CO_2} calc	y_{CO_2} calc
3.38	0.2074	0.1991	0.9914	0.2313	0.9909	0.1724	0.9930	0.1831	0.9932
4.74	0.3097	0.2972	0.9923	0.3356	0.9916	0.2746	0.9943	0.2868	0.9946
5.98	0.4110	0.4140	0.9921	0.4478	0.9911	0.4198	0.9949	0.4203	0.9952
6.73	0.5014	0.5237	0.9915	0.5373	0.9902	0.5728	0.9950	0.5459	0.9954
7.14	0.6109	0.6320	0.9909	0.6087	0.9892	0.6730	0.9950	0.6489	0.9954
7.27	0.7095	0.6863	0.9906	0.6417	0.9888	0.7021	0.9949	0.6905	0.9954
7.53	0.8072	0.8121	0.9901	0.8258	0.9878	0.7547	0.9949	0.7946	0.9955

x_{CO_2}: liquid phase molar fraction.
y_{CO_2}: vapor phase molar fraction.

Table 9: VLE data at 318.2 K.

318.2 K									
*P*exp (MPa)		PR-MKP		PR quadratic		SAFT-ConvexBody		Conventional SAFT	
	x_{CO_2} exp	x_{CO_2} calc	y_{CO_2} calc	x_{CO_2} calc	y_{CO_2} calc	x_{CO_2} calc	y_{CO_2} calc	x_{CO_2} calc	y_{CO_2} calc
3.65	0.2074	0.2009	0.9892	0.2232	0.9887	0.1736	0.9915	0.1822	0.9917
5.12	0.3097	0.2992	0.9901	0.3272	0.9893	0.2759	0.9930	0.2850	0.9933
6.45	0.4110	0.4125	0.9895	0.4392	0.9885	0.4177	0.9935	0.4149	0.9939
7.30	0.5014	0.5195	0.9883	0.5334	0.9868	0.5719	0.9935	0.5424	0.9941
7.78	0.6109	0.6244	0.9870	0.6114	0.9851	0.6740	0.9934	0.6498	0.9940
7.97	0.7095	0.6956	0.9863	0.6596	0.9841	0.7102	0.9933	0.7043	0.9940
8.21	0.8072	0.8099	0.9853	0.8220	0.9823	0.7513	0.9932	0.7885	0.9939

x_{CO_2}: liquid phase molar fraction.
y_{CO_2}: vapor phase molar fraction.

Table 10: VLE at 323.2 K.

323.2 K									
*P*exp (MPa)		PR-MKP		PR quadratic		SAFT-ConvexBody		Conventional SAFT	
	x_{CO_2} exp	x_{CO_2} calc	y_{CO_2} calc	x_{CO_2} calc	y_{CO_2} calc	x_{CO_2} calc	y_{CO_2} calc	x_{CO_2} calc	y_{CO_2} calc
3.88	0.2074	0.1954	0.9869	0.2260	0.9862	0.1717	0.9896	0.1821	0.9899
5.48	0.3097	0.2942	0.9878	0.3314	0.9870	0.2735	0.9914	0.2855	0.9918
6.97	0.4110	0.4127	0.9869	0.4456	0.9856	0.4166	0.9919	0.4179	0.9925
8.03	0.5014	0.5446	0.9848	0.5514	0.9827	0.5911	0.9917	0.5632	0.9925
8.42	0.6109	0.6262	0.9833	0.6052	0.9806	0.6643	0.9914	0.6400	0.9923
8.61	0.7095	0.6811	0.9824	0.6393	0.9791	0.6971	0.9913	0.6847	0.9922
8.99	0.8072	0.8119	0.9796	0.8150	0.9740	0.7547	0.9908	0.7995	0.9918

x_{CO_2}: liquid phase molar fraction.
y_{CO_2}: vapor phase molar fraction.

Table 11: Bubble pressure experimental (BPexp) versus calculated at 298.2 K.

BPexp (MPa)	x_{CO_2} exp	PR-MKP		PR quadratic		SAFT-ConvexBody		Conventional SAFT	
		BPcalc (MPa)	ARD	BPcalc (MPa)	ARD	BPcalc (MPa)	ARD	BPcalc (MPa)	ARD
2.79	0.2078	2.59	0.0720	2.47	0.1154	3.12	0.1195	3.02	0.0828
3.88	0.3094	3.71	0.0427	3.57	0.0802	4.05	0.0439	3.98	0.0264
4.67	0.4117	4.63	0.0090	4.50	0.0370	4.65	0.0035	4.65	0.0036
5.14	0.5108	5.23	0.0177	5.15	0.0027	5.02	0.0228	5.08	0.0107
5.44	0.6110	5.54	0.0178	5.52	0.0148	5.28	0.0280	5.37	0.0132
5.62	0.7093	5.62	0.0002	5.62	0.0001	5.53	0.0157	5.55	0.0119
5.64	0.8074	5.64	0.0000	5.61	0.0046	5.82	0.0319	5.69	0.0084

x_{CO_2}: liquid phase molar fraction.
y_{CO_2}: vapor phase molar fraction.

Table 12: Bubble pressure experimental (BPexp) versus calculated at 313.2 K.

BPexp (MPa)	x_{CO_2} exp	PR-MKP		PR quadratic		SAFT-ConvexBody		Conventional SAFT	
		BPcalc (MPa)	ARD	BPcalc (MPa)	ARD	BPcalc (MPa)	ARD	BPcalc (MPa)	ARD
3.38	0.2074	3.50	0.0369	3.05	0.0981	3.90	0.1529	3.73	0.1043
4.74	0.3097	4.89	0.0316	4.41	0.0688	5.10	0.0700	4.99	0.0524
5.98	0.4110	5.96	0.0037	5.61	0.0619	5.93	0.0089	5.91	0.0112
6.73	0.5014	6.61	0.0180	6.46	0.0403	6.42	0.0458	6.50	0.0339
7.14	0.6109	7.08	0.0085	7.15	0.0014	6.88	0.0360	7.00	0.0189
7.27	0.7095	7.32	0.0066	7.43	0.0221	7.30	0.0047	7.32	0.0074
7.53	0.8072	7.52	0.0014	7.51	0.0020	7.83	0.0401	7.56	0.0034

x_{CO_2}: liquid phase molar fraction.
y_{CO_2}: vapor phase molar fraction.

Table 13: Bubble pressure experimental (BPexp) versus calculated at 318.2 K.

BPexp (MPa)	x_{CO_2} exp	PR-MKP		PR quadratic		SAFT-ConvexBody		Conventional SAFT	
		BPcalc (MPa)	ARD	BPcalc (MPa)	ARD	BPcalc (MPa)	ARD	BPcalc (MPa)	ARD
3.65	0.2074	3.76	0.0288	3.41	0.0653	4.19	0.1474	4.05	0.1088
5.12	0.3097	5.26	0.0271	4.89	0.0455	5.50	0.0746	5.41	0.0571
6.45	0.4110	6.43	0.0024	6.14	0.0472	6.40	0.0070	6.42	0.0045
7.30	0.5014	7.18	0.0159	7.04	0.0352	6.95	0.0387	7.07	0.0320
7.78	0.6109	7.73	0.0574	7.78	0.0380	7.48	0.0006	7.62	0.0020
7.97	0.7095	8.00	0.0038	8.09	0.0151	7.96	0.0465	7.98	0.0019
8.21	0.8072	8.20	0.0008	8.20	0.0352	8.59	0.0474	8.25	0.0055

x_{CO_2}: liquid phase molar fraction.
y_{CO_2}: vapor phase molar fraction.

Homogenization of the mixture is guaranteed by a small magnetic bar and an external magnetic stirrer. The cell is enclosed by an electric mantle and an automatic control system that keeps the temperature constant. The pressure is measured by a calibrated pressure transducer (GEFRAN model TK-E-1-E-B35D-H-V) with uncertainty of ±0.01 MPa.

The ultra-sound wave is generated by a pair of US transducers (General Electric model MB4S 57749, frequency of 4 MHz, and diameter of 10 mm) connected externally to the cell by means of a thread. Each transductor is connected to a plate (MATEC SR9000), installed in the microcomputer, which is responsible for the emissions and captures of the ultrasonic waves. The ultra-sound emissor transducer captures the electric signal sent by the computer and converts it into an ultrasonic wave at the desired frequency. Afterwards, the ultra-sound receptor transducer captures the ultrasonic wave that was propagated through the fluid under investigation and converts it into an electric signal. Both waves are analyzed in real time in the oscilloscope, and the distance between the pair of transductors, which is fixed and known, corresponds to the path of the ultrasonic wave.

The amplitude of the wave is observed through a digital oscilloscope (Tektronix model 1001B, with two channels), which monitors the acoustic waves transmitted and captured by the pair of channels separately and simultaneously. The time difference between the beginning of the transmission of the pulse and the beginning of the capture of the signal by the receptor transducer is used to calculate the sound velocity in the fluid under the specified conditions of pressure and temperature. The external indicator of the oscilloscope monitores the plate which generates the signals so that the synchronism of the actions is guaranteed.

The technique employed to carry out the vapor-liquid equilibrium measurements is based on the synthetic method that prevents sampling and analysis of both phases. In an evacuated cell, ethanol is added through a syringe. The mass of the syringe is measured in an analytic balance (TOLEDO model Adventurer Ohaus) with uncertainty of ±0.001 g before and after the injection to know the exacted mass of ethanol present in the cell. Carbon dioxide is transferred at constant temperature and pressure (288.2 K and 10.00 MPa) into the pump cylinder and then fed into the cell, in liquid phase, using a syringe pump (ISCO model 260D) that controls the volume of carbon dioxide in its cylinder. The pump cylinder has a jacket, where water at 288.2 K is circulated from a thermobath. Under these conditions (288.2 K and 10.00 MPa), CO_2 density is 0.8901 (http://webbook.nist.gov). In this way, the amount of carbon dioxide is known with ±0.01 mL of precision. After the filling operation, the precise composition of the binary mixture can be calculated. The temperature of the system is set to the desired value. When this value is reached, the pressure of the mixture is slowly increased by the piston motion until the system becomes homogeneous (liquid phase). When the thermal equilibrium in the one-phase region is reached, the pressure is slowly decreased with a programmed rate until the first bubble is observed. The phase boundary is located in the

Table 14: Bubble pressure experimental (BPexp) versus calculated at 323.2 K.

BPexp (MPa)	x_{CO_2}exp	PR-MKP		PR quadratic		SAFT-ConvexBody		Conventional SAFT	
		BPcalc (MPa)	ARD	BPcalc (MPa)	ARD	BPcalc (MPa)	ARD	BPcalc (MPa)	ARD
3.88	0.2074	4.09	0.0540	3.58	0.0773	4.50	0.1592	4.31	0.1108
5.48	0.3097	5.70	0.0399	5.16	0.0582	5.93	0.0823	5.79	0.0572
6.97	0.4110	6.96	0.0020	6.56	0.0593	6.93	0.0059	6.91	0.0086
8.03	0.5014	7.75	0.0350	7.57	0.0568	7.54	0.0604	7.64	0.0486
8.42	0.6109	8.36	0.0073	8.45	0.0042	8.13	0.0340	8.28	0.0163
8.61	0.7095	8.70	0.0099	8.86	0.0292	8.68	0.0088	8.70	0.0110
8.99	0.8072	8.98	0.0015	8.98	0.0006	9.41	0.0465	9.02	0.0029

x_{CO_2}: liquid phase molar fraction.
y_{CO_2}: vapor phase molar fraction.

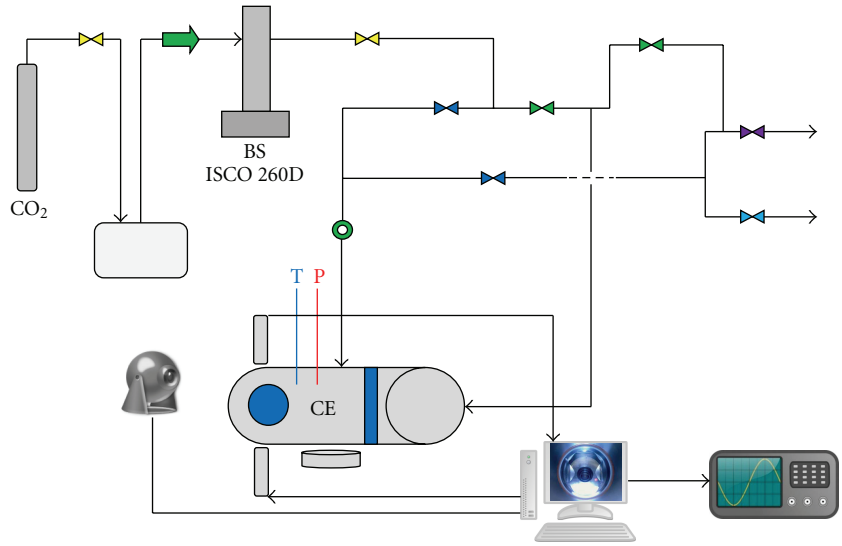

Figure 3: Ultrasonic and visual VLE apparatus: CO_2: CO_2 cylinder; BS ISCO 260D: syringe pump ISCO 260 D; CE: high-pressure variable volume cell; T: temperature system indicator/controller; P: pressure transducer; webcam/computer/monitor/oscilloscope.

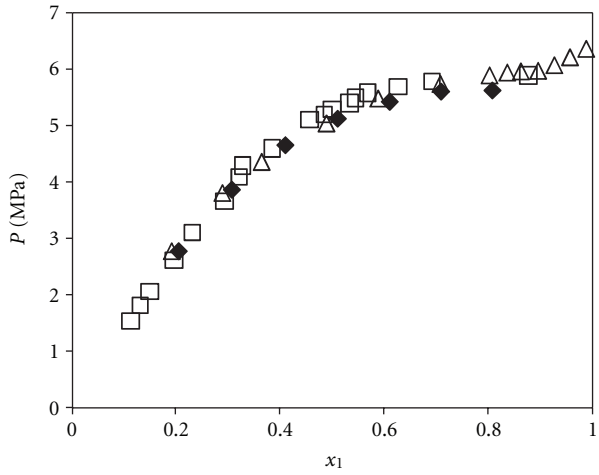

Figure 4: Bubble pressure curve versus liquid phase molar fraction of the system carbon dioxide (1) + ethanol (2) at 298.15 K. Symbols, experimental data: □ Kordikowski et al. [7], ♦ present work (acoustic method), Δ Chiu et al. [9].

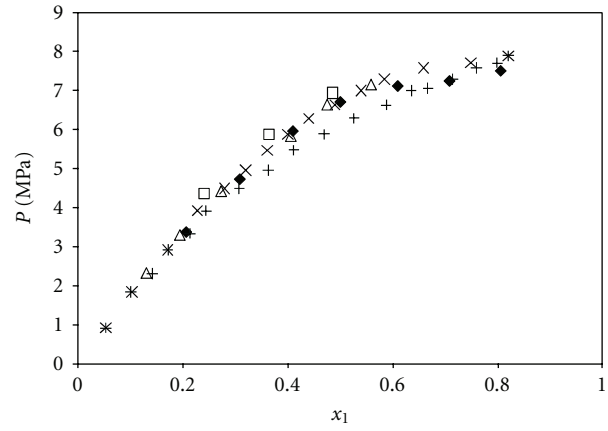

Figure 5: Bubble pressure curve versus liquid phase molar fraction of the system carbon dioxide (1) + ethanol (2) at 313.2 K. Symbols, experimental data: Δ Secuianu et al. [8], ♦ present work (acoustic method), □ Stievano and Elvassore [10], × Chang et al. [11], + Day et al. [12].

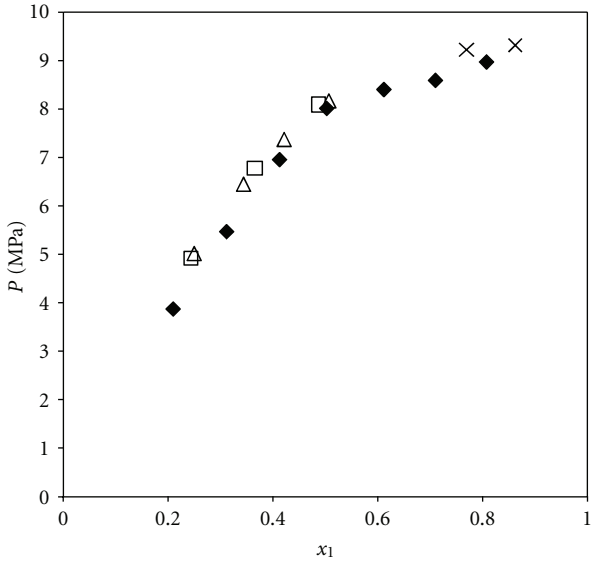

Figure 6: Bubble pressure curve versus liquid phase molar fraction of the system carbon dioxide (1) + ethanol (2) at 323.2 K. Symbols, experimental data: Δ Chen et al. [13], ♦ present work (acoustic method), □ Stievano and Elvassore [10], × Yeo et al. [14].

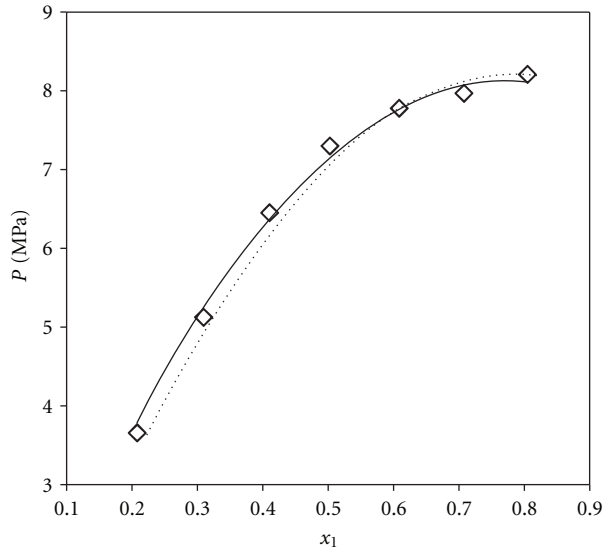

Figure 7: Bubble pressure curve *versus* liquid phase molar fraction of the system carbon dioxide (1) + ethanol (2) at 318.15 K. Experimental data (present work): ◊; solid line: calculations using PR-MKP; dashed line: calculations using PR quadratic.

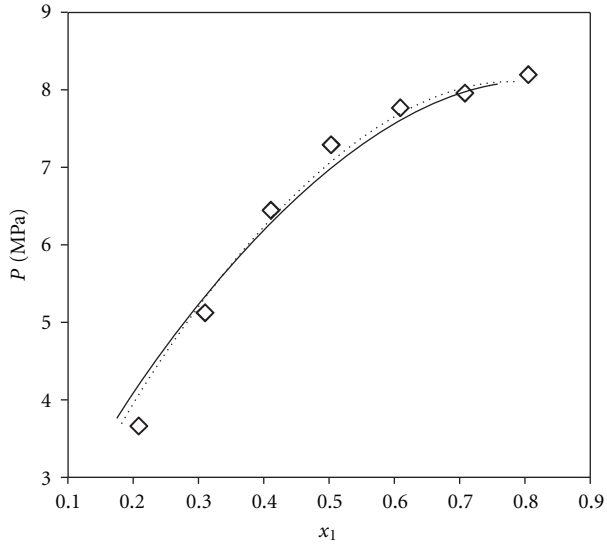

Figure 8: Bubble pressure curve *versus* liquid phase molar fraction of the system carbon dioxide (1) + ethanol (2) at 318.15 K. Experimental data (present work): ◊; solid line: calculations using SAFT-ConvexBody; dashed line: calculations using Conventional SAFT.

pressure interval between the points where it is possible to distinguish between a single, and a two-phase state. The size of the pressure interval is reduced by alternately increasing and decreasing the pressure a couple of times (at least two) each time viewing the phase change in the computer monitor and the decrease of US signal amplitude in the oscilloscope to determine the bubble pressure. The composition of the major phase (liquid phase at bubble point) is taken as being the overall composition into the cell. The liquid phase compositions (mass fractions) were estimated to be precision within ±0.01.

4. Experimental Results

The equipment used and the procedure adopted were validated by comparing the results obtained for the VLE data for the system carbon dioxide + ethanol at 298.2 K (Figure 4), 313.2 K (Figure 5), and 323.2 K (Figure 6) with those reported by other authors at the same temperature. Figure 4 presents the data obtained in this work and literature data [7, 9], which used the sampling and the visual technique, respectively. Figure 5 shows the data obtained in this work and the literature data [8, 10], which used the sampling and the visual techniques, respectively. Figure 6 presents the data obtained in this work and the literature data [10, 13, 14], which used the visual, sampling, and visual techniques, respectively. The results of the present work were found to be in agreement with these authors.

The experimental apparatus allows the phase transition detection via visual and acoustic methods simultaneously. The results at 298.2 K are listed in Table 1. A good agreement was observed between both methods, for a set of seven molar fractions, with average absolute deviation in bubble pressure of ±0.01 MPa. It is important to note that this system, in the range of compositions considered, exhibits good transparency so that the visual observation of the phase transition is rather easy.

The bubble pressures of the system carbon dioxide + ethanol at three temperatures obtained in the present study are given in Table 2 along with the corresponding standard deviations. The results are the average of at least three different measurements.

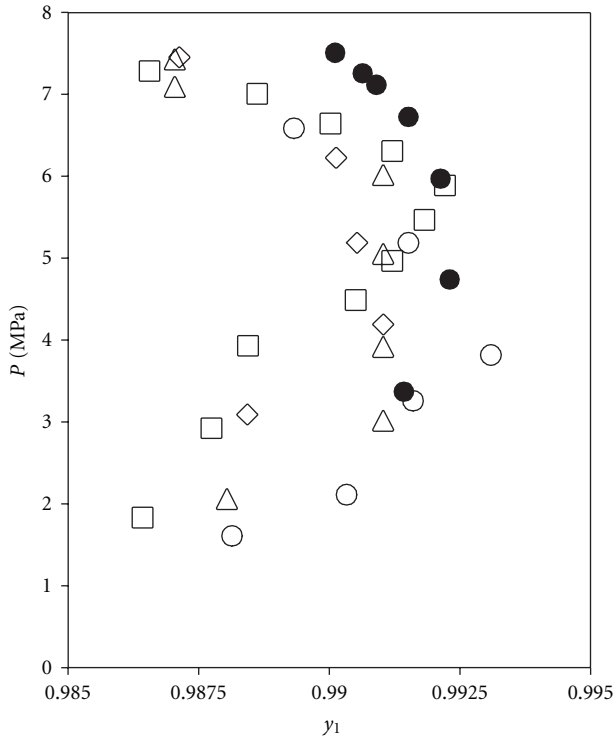

Figure 9: Pressure *versus* vapor phase molar fraction curve (*P-y*) of carbon dioxide (1) + ethanol (2) at 313.15 K. Comparison between data from the literature and calculated with PR-MKP. Symbols: □ Day et al. [12]; △ Suzuki et al. [15]; ● present work; ○ Tsivintzelis et al. [16]; ◊ Galicia-Luna et al. [17].

5. Thermodynamic Modeling

The mixture under investigation in this study, carbon dioxide + ethanol, exhibits a highly nonideal behavior not only regarding the nature of both components, but also at the high pressures involved. Thus, the prediction of the VLE behavior requires the use of reliable and powerful thermodynamic models. Cubic equations of state and equations of state that directly account for associations like hydrogen bonds were chosen for the modeling.

The experimental VLE data were correlated with Peng-Robinson equation of state [18] combined with two different mixing rules: van der Waals quadratic and Mathias-Klotz-Prausnitz [19] (MKP). The original SAFT equation of state [20] (Conventional SAFT) and one of its modifications, SAFT-ConvexBody [21], were also used in the modeling. SAFT-ConvexBody, based on the thermodynamic statistics, is claimed as being able to represent satisfactorily the VLE of systems at temperatures slightly above the critical point of one of the components, which is typically found in processes of supercritical extractions. Conventional SAFT uses van der Waals quadratic mixing rules combined with MKP mixing rules. SAFT-ConvexBody [21] uses a mixing rule, based on segments of molecules, that combines the van der Waals quadratic with MKP mixing rules.

The details and further information regarding the equations of state, mixing rules and corresponding binary interaction parameters employed for this modeling can be found in the mentioned-above references [18–21]. All these equations of state and the mixing rules are available in the software PE 2000 [22], which was used to perform the VLE calculations in this work.

The Peng-Robinson equation of state requires only the critical constants and the acentric factor to calculate the pure component parameters used in this modeling. These constants for the components of interest in this study were retrieved from PE 2000 database. The Conventional SAFT and SAFT-ConvexBody equations of state require specific parameters of each pure component of the mixture. They are obtained by fitting experimental data of vapor pressure and saturated liquid volume. For ethanol and carbon dioxide, such parameters were retrieved from PE 2000 and are shown in Table 3. Additionally, the association scheme must be specified. In the case of ethanol two association sites per molecule, representing the hydrogen bonds, were chosen.

The experimental determination of the bubble points curve for the system carbon dioxide + ethanol was performed at four temperatures: 298.2 K, 313.2 K, 318.2 K, and 318.2 K, starting from the overall molar fractions previously determined. The binary interaction parameters for each equation of state were determined from the best fit of calculated and experimental isothermal *P-x* data. The objective function chosen in the PE 2000 is written in terms of the relative quadratic deviations of the liquid mol fractions, because only the liquid phase composition was measured in this study. The binary interaction parameters of the SAFT and Peng-Robinson equations of state are listed in Tables 4 and 5, respectively.

A weak dependence of the binary interaction parameters on the temperature was observed in the interval of temperatures from 313.2 K to 323.2 K, especially for the SAFT-ConvexBody and Conventional SAFT. Nevertheless, the effect of the temperature on the parameters cannot be neglected if the results obtained at 298.2 K are included in the comparison. The influence of temperature was found to be higher for the Peng-Robinson cubic equation of state, with both mixing rules, than for the SAFT equations of state.

The prediction of the molar fractions of the liquid phase and the bubble pressure (BP) by each equation of state was then carried out using the optimized binary parameters. Table 6 presents the percent average relative deviations (ARD) of liquid molar fractions and BP obtained at each isotherm for seven data experimental points. The ARD of carbon dioxide in the liquid phase varies from 2.1% to 9.3%, whereas the ARD in BP ranges from 1.5% to 5.7%. Based on the ARD criterium, the best performance was achieved with Peng Robinson/Mathias-Klotz-Prausnitz (PR-MKP) and Conventional SAFT, which led to lowest deviation. PR-MKP yielded the best results for all temperatures, except 298.2 K at which Conventional SAFT performed slightly better. The performance of SAFT-ConvexBody was not as good as PR-MKP and Conventional SAFT. It might perform better at low solute concentration, a common condition in supercritical extractions, which lies outside the composition range used in this study.

The performance of the four models used in this work can be observed in Figures 5 and 6 that present *P-x* curves

with experimental and calculated data at 318.2 K, which represent a new set of VLE experimental data for carbon dioxide + ethanol. These plots confirm that both the cubic and the SAFT type equations of state were able to reproduce rather correctly the experimental data within the composition range. According to Figure 7, PR-MPK proved to be suitable for this system, while PR with the quadratic mixing did not show good results. Both SAFT equations of state performed similarly, as presented in Figure 8. The chosen models were expected to perform satisfactorily based on their theoretical foundations, especially SAFT. However, depending on the composition range and temperature of the system a rather simple cubic equation of state Peng-Robinson combined with a more powerful empirical mixing rule, MKP, was found to represent rather correctly the experimental data.

In order to evaluate the capability of the modeling in calculating the molar fractions in the vapor phase, the results obtained with the equation of state, which yielded the best results for the liquid composition, were compared with some experimental data taken from the literature. The performance of the PR-MKP at 313.2 K is illustrated in Figure 9, which shows plots of pressure versus vapor molar fraction of carbon dioxide. Vapor phase experimental data at this temperature are available in the literature [12, 15–17]. Although the pressure and composition ranges at 313.2 K are not very similar, *P-y* data from these studies were plotted along with the values predicted by PR-MKP. It is clear that the model overestimates the mol fractions of carbon dioxide above 6.00 MPa and, consequently, underpredicts the solubility of ethanol in the supercritical carbon dioxide. However, the differences between the predicted values and the closest corresponding experimental data are small and may be less than the average precision estimated for the vapor compositions. Compared with the experimental data [15], for instance, the differences of the vapor compositions were found to be within ±0.4%, whereas the precision of the vapor composition reported by the author is estimated to be ±1%. As far as the solubility of ethanol in the supercritical carbon dioxide at 318.2 K is concerned, the closest isotherm with vapor molar fraction experimentally obtained, found in the literature, is 314.8 K [23]. The results of this study (vapor phase mole fraction of ethanol) with PR-MKP at 318 K vary from 0.0099 to 0.0147.

The results of the modeling are summarized in the Tables 7, 8, 9, and 10, which displays the calculated va and liquid compositions at all isotherms investigated in this work. Tables 11, 12, 13, and 14 contain the calculated BP along with the relative deviations compared with the experimental values.

6. Conclusions

The phase equilibrium behavior of the binary system carbon dioxide + ethanol was investigated via the synthetic methodology using both the acoustic and the visual methods at 298.2 K, 313.2 K, 318.2 K, and 323.2 K with pressures ranging from 3.0 MPa to 9.0 MPa. The apparatus assembled for measuring VLE at high pressure combining the visual with the acoustic methods showed satisfactory performance with results similar to those reported in the open literature. The modeling of the measured VLE data revealed that both cubic equations of state and SAFT approaches represent satisfactorily the behavior of the binary system, but the results with Peng-Robinson equation of state using the MKP mixing rule were the best.

Acknowledgment

The authors would like to thank ANP (PRH-13), CNPq, and FAPERJ for financial support.

References

[1] A. Kordikowski and M. Poliakoff, "Acoustic probing of phase equilibria in near-critical fluids," *Fluid Phase Equilibria*, vol. 150, no. 151, pp. 493–499, 1998.

[2] H. Carrier, F. Plantier, J. L. Daridon, B. Lagourette, and Z. Lu, "Acoustic method for measuring asphaltene flocculation in crude oils," *Journal of Petroleum Science & Engineering*, vol. 27, no. 3-4, pp. 111–117, 2000.

[3] Z. Lu, J. L. Daridon, B. Lagourette, and S. Ye, "Phase comparison technique for measuring liquid-liquid phase equilibrium," *Review of Scientific Instruments*, vol. 70, no. 4, pp. 2065–2068, 1999.

[4] G. Madras, C. Kolluru, and R. Kumar, "Synthesis of biodiesel in supercritical fluids," *Fuel*, vol. 83, no. 14-15, pp. 2029–2033, 2004.

[5] J. M. Dobbs, J. M. Wong, R. J. Lahiere, and K. P. Johnston, "Modification of supercritical fluid phase behavior using polar cosolvents," *Industrial and Engineering Chemistry Research*, vol. 26, no. 1, pp. 56–65, 1987.

[6] C. Garlapati and G. Madras, "Solubilities of hexadecanoic and octadecanoic acids in supercritical CO_2 with and without cosolvents," *Journal of Chemical & Engineering Data*, vol. 53, no. 12, pp. 2913–2917, 2008.

[7] A. Kordikowski, A. P. Schenk, R. M. van Nielen, and C. J. Peters, "Volume expansions and vapor-liquid equilibria of binary mixtures of a variety of polar solvents and certain near-critical solvents," *The Journal of Supercritical Fluids*, vol. 8, no. 3, pp. 205–216, 1995.

[8] C. Secuianu, V. Feroiu, and D. Geană, "Phase behavior for carbon dioxide + ethanol system: experimental measurements and modeling with a cubic equation of state," *The Journal of Supercritical Fluids*, vol. 47, no. 2, pp. 109–116, 2008.

[9] H. Y. Chiu, M. J. Lee, and H. M. Lin, "Vapor-liquid phase boundaries of binary mixtures of carbon dioxide with ethanol and acetone," *Journal of Chemical & Engineering Data*, vol. 53, no. 10, pp. 2393–2402, 2008.

[10] M. Stievano and N. Elvassore, "High-pressure density and vapor-liquid equilibrium for the binary systems carbon dioxide-ethanol, carbon dioxide-acetone and carbon dioxide-dichloromethane," *The Journal of Supercritical Fluids*, vol. 33, no. 1, pp. 7–14, 2005.

[11] C. J. Chang, C. Y. Day, C. M. Ko, and K. L. Chiu, "Densities and P-x-y diagrams for carbon dioxide dissolution in methanol, ethanol, and acetone mixtures," *Fluid Phase Equilibria*, vol. 131, no. 1-2, pp. 243–258, 1997.

[12] C.-Y. Day, C. J. Chang, and C.-Y. Chen, "Phase equilibrium of ethanol + CO_2 and acetone + CO_2 at elevated pressures,"

Journal of Chemical & Engineering Data, vol. 44, no. 2, p. 365, 1999.

[13] H. I. Chen, H. Y. Chang, E. T. S. Huang, and T. C. Huang, "A new phase behavior apparatus for supercritical fluid extraction study," *Industrial and Engineering Chemistry Research*, vol. 39, no. 12, pp. 4849–4852, 2000.

[14] S. D. Yeo, S. J. Park, J. W. Kim, and J. C. Kim, "Critical properties of carbon dioxide+methanol, +ethanol, +1-propanol, and +1-butanol," *Journal of Chemical & Engineering Data*, vol. 45, no. 5, pp. 932–935, 2000.

[15] K. Suzuki, H. Sue, M. Itou et al., "Isothermal vapor-liquid equilibrium data for binary systems at high pressures: carbon dioxide-methanol, carbon dioxide-ethanol, carbon dioxide-1-propanol, methane-ethanol, methane-1-propanol, ethane-ethanol, and ethane-1-propanol systems," *Journal of Chemical & Engineering Data*, vol. 35, no. 1, pp. 63–66, 1990.

[16] I. Tsivintzelis, D. Missopolinou, K. Kalogiannis, and C. Panayiotou, "Phase compositions and saturated densities for the binary systems of carbon dioxide with ethanol and dichloromethane," *Fluid Phase Equilibria*, vol. 224, no. 1, pp. 89–96, 2004.

[17] L. A. Galicia-Luna, A. Ortega-Rodriguez, and D. Richon, "New apparatus for the fast determination of high-pressure vapor-liquid equilibria of mixtures and of accurate critical pressures," *Journal of Chemical & Engineering Data*, vol. 45, no. 2, pp. 265–271, 2000.

[18] D. Y. Peng and D. B. Robinson, "A new two-constant equation of state," *Industrial & Engineering Chemistry Fundamentals*, vol. 15, no. 1, pp. 59–64, 1976.

[19] P. M. Mathias, H. C. Klotz, and J. M. Prausnitz, "Equation-of-state mixing rules for multicomponent mixtures: the problem of invariance," *Fluid Phase Equilibria*, vol. 67, pp. 31–44, 1991.

[20] S. H. Huang and M. Radosz, "Equation of state for small, large, polydisperse, and associating molecules," *Industrial and Engineering Chemistry Research*, vol. 29, no. 11, pp. 2284–2294, 1990.

[21] O. Pfohl and G. Brunner, "2. Use of BACK to modify SAFT in order to enable density and phase equilibrium calculations connected to gas-extraction processes," *Industrial and Engineering Chemistry Research*, vol. 37, no. 8, pp. 2966–2976, 1998.

[22] S. Petkov, O. Pfhol, and G. Brunner, "PE 2000—a powerful tool to correlate phase equilibria," Fev. 2000, http://www.tu-harburg.de/alt/v8/prof-smirnova/publications/pe-2000.html.

[23] D. W. Jennings, R. J. Lee, and A. S. Teja, "Vapor-liquid equilibria in the carbon dioxide + ethanol and carbon dioxide + 1-butanol systems," *Journal of Chemical & Engineering Data*, vol. 36, no. 3, pp. 303–307, 1991.